This document is downloaded from DR-NTU (https://dr.ntu.edu.sg)
Nanyang Technological University, Singapore.

High-k, ultrastretchable self-enclosed ionic liquid-elastomer composites for soft robotics and flexible electronics

Ankit; Tiwari, Naveen; Ho, Fanny; Krisnadi, Febby; Kulkarni, Mohit Rameshchandra; Nguyen, Linh Lan; Koh, Adrian Soo Jin; Mathews, Nripan

2020

Ankit, Tiwari, N., Ho, F., Krisnadi, F., Kulkarni, M. R., Nguyen, L. L., Koh, A. S. J. & Mathews, N. (2020). High-k, ultrastretchable self-enclosed ionic liquid-elastomer composites for soft robotics and flexible electronics. ACS Applied Materials and Interfaces, 12(33), 37561-37570. https://dx.doi.org/10.1021/acsami.0c08754

https://hdl.handle.net/10356/152973

https://doi.org/10.1021/acsami.0c08754

This document is the Accepted Manuscript version of a Published Work that appeared in final form in ACS Applied Materials and Interfaces, copyright © American Chemical Society after peer review and technical editing by the publisher. To access the final edited and published work see https://doi.org/10.1021/acsami.0c08754.

Downloaded on 13 Mar 2024 17:06:44 SGT

SUPPORTING INFORMATION

High-k, Ultra-Stretchable Self-Enclosed Ionic Liquid-Elastomer Composites for Soft Robotics and Flexible Electronics

*Ankit, Naveen Tiwari, Fanny Ho, Febby Krisnadi, Mohit Rameshchandra Kulkarni, Linh Lan Nguyen, Soo Jin Adrian Koh, Nripan Mathews**

*Corresponding author: Nripan@ntu.edu.sg

Basic configuration of Dielectric elastomer actuators (DEAs)

DEA, in their simplest configuration, resemble a variable capacitor with an elastomeric layer sandwiched between compliant electrodes on either side (Figure S1). The relationship of material parameters and operating conditions with actuation performance for DEAs can be broadly understood with the help of following equations, where p is the electrostatic stress, ε_r is the relative permittivity (dielectric constant) of the elastomer, ε_o is the permittivity of vacuum, V is the applied voltage, d is the thickness of the elastomer, S is the actuation strain produced in the thickness direction, and Y is the Young's modulus of the elastomer.

$$p = \varepsilon_r \varepsilon_o ({}^{V}/_{d})^2 \quad (1)$$

$$S = {}^{p}/_{Y} = \varepsilon_r \varepsilon_o ({}^{V}/_{d})^2 ({}^{1}/_{Y}) \quad (2)$$

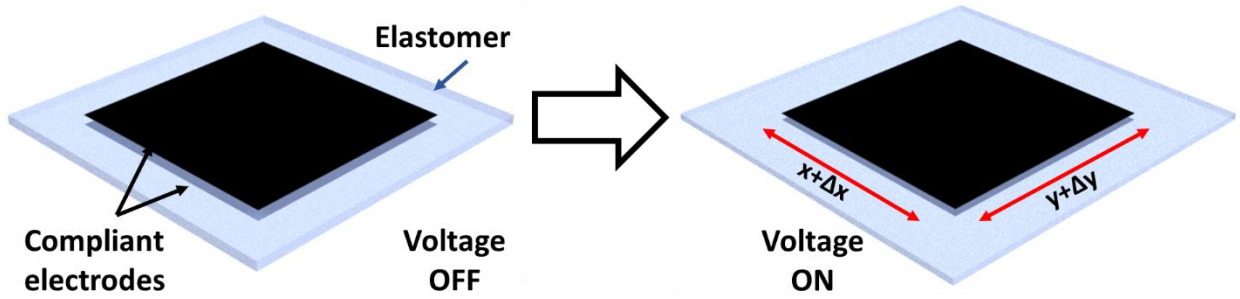

Figure S1. Basic configuration of a dielectric elastomer actuator (DEA). DEA resembles a compliant capacitor in its architecture, with an elastomeric layer sandwiched between two compliant electrodes. Upon application of voltage, electric field induces charges on opposing sides and resulting electrostatic force induces stress in soft material.

Effective medium theories for dielectric approximation

Maxwell-Garnett approximation is one of the earliest and preferred effective medium theories for effective permittivity approximations. The model assumes a two-phase isotropic dielectric component with spherical inclusions ideally dispersed, and defines the effective relative permittivity as given by equation (3). ε_c is the effective dielectric constant of the composite, ε_1 is the dielectric constant of the matrix, ε_2 is the dielectric constant of the filler material and v_2 is the loading of the filler particle.

$$\varepsilon_c = \varepsilon_1 \left[1 + {3v_2(\varepsilon_2 - \varepsilon_1)} \Big/ {2\varepsilon_1 + \varepsilon_2 - v_2(\varepsilon_2 - \varepsilon_1)}\right] \quad (3)$$

However, the model is not accurate for drastic difference in dielectric constants and provides anomalous results for highly polarizable inclusions. Bruggeman's model is an extension of the Maxwell-Garnett approximation. This model allows the computation of the overall electrical response of the composite at high loading contents of the high-k fillers, with the assumptions that the dispersed fillers are spherical in shape and the dispersions do not create a percolative path through the medium. The model encompasses the polarizability of the inclusions in the calculation and is given by the following mathematical expression (equation (4)).

$$\varepsilon_c = \varepsilon_2 \left[{3\varepsilon_1 + 2v_2(\varepsilon_2 - \varepsilon_1)} \Big/ {3\varepsilon_2 - v_2(\varepsilon_2 - \varepsilon_1)}\right] \quad (4)$$

Yamada's model, a more accurate approximation model, is based on the assumption that the polymer dielectric characteristics are quite distinct from the dielectric characteristics of the filler. The model also introduces a shape parameter "n" for non-spherical inclusions in the polymer matrix. "n" is a geometry factor and is given a value of 3 for spherical particles. "n" < 3 corresponds to oblate particles, whereas n > 3 corresponds to prolate particles in the applied electric field (equation (5)).

$$\varepsilon_c = \varepsilon_1 \left[1 + {nv_2(\varepsilon_2 - \varepsilon_1)} \Big/ {n\varepsilon_1 + (1 - v_2)(\varepsilon_2 - \varepsilon_1)}\right] \quad (5)$$

Figure 2a shows the plot of dielectric constant values of our EMIMTFSI-PDMS system approximated from the Bruggeman's model and the Yamada's model at different frequencies. The dielectric constant values for baseline matrix were measured by dielectric spectroscopy of PDMS. The static dielectric constant value of EMIMTFSI (12.25) was taken from literature for the approximations. For Yamada's model, the value of n was allotted as 3, for spherical particles of IL were observed in the PDMS matrix. This was later confirmed by optical microscopy images as well. The values were approximated at a 20% filler loading by volume.

Eshelby's theory and its extensions for liquid inclusions in solid matrix

Eshelby's theory lays down the foundation for composite mechanics through the description of strain response of segregated inclusions to applied stresses in a composite. It helps to predict the stiffness of solid composites consisting of low volume fraction of inclusions. According to Eshelby's result, liquid inclusions with zero Young's modulus should lower the resulting stiffness of the solid composites. Mathematical expression for Eshelby's theory for dilute composites is given by equation (6). Y_c represents the effective moduli of the composite, Y stands for the Young's modulus of the matrix and ϕ is the volume loading of the inclusions.

$$Y_c = {Y}/{1 + ({5}/{3})\emptyset} \tag{6}$$

However, the theory only holds true for very dilute composites, and does not incorporate the physics of interfaces in the approximation. Mori-Tanaka approximation scheme extends the theory for treating non-dilute composites, which is based on the concept of equivalent inclusion and average stress in the matrix. Nonetheless, both the approximation do not take interfacial thermodynamics into account. And as is the case, when the inclusions become very small, the surface energy becomes important compared to the bulk strain energy and the interfacial effects cannot be ignored. Surface tension (Υ), which typically acts to smooth our interfaces, plays an important role when the inclusions become small and keeps liquid inclusions from deforming against applied stretch. Style et. al. included the interfacial effects into their model for effective modulus approximations; and is given by equation (7) as extension of Mori-Tanaka approximation scheme and equation (8) as extension of Eshelby's theory. It is important to note that the model is developed based on the assumption that surface tension is independent of surface strain, which does not hold true in general. Additionally, it is worthwhile to mention that the experimental validation of all the models has been done by force-indentation measurements and not uniaxial tensile tests. Y_c represents the effective moduli of the composite, Y stands for the Young's modulus of the matrix, ϕ is the volume loading of the inclusions, R is the radius

of the liquid inclusion, L denotes the elastocapillary length (given by L=ϒ/Y), ϒ is the surface tension, and Y_i denotes the approximated moduli of the liquid inclusions (given by $Y_i = 12\Upsilon/5R$).

$$Y_c/Y = \left(15 + 9\emptyset + (R/L)(6 - 6\emptyset)\right) / \left(15 - 6\emptyset + (R/L)(6 + 4\emptyset)\right) \quad (7)$$

$$Y_c/Y = \left(1 + (2/3)(Y_i/Y)\right) / \left((2/3 - 5/3\,\emptyset)(Y_i/Y) + (1 + 5/3\,\emptyset)\right) \quad (8)$$

Figure 2b shows the plot of Young's modulus of composite approximated from equation (7), which represents Style et. al.'s extension of Mori-Tanaka approximation scheme for non-dilute composites. Surface tension (ϒ) value is taken as 44.14 mN/m from the literature for the modeling. Value of R was taken as 1μm, which was the average radii of liquid inclusions. Reduction of Young's modulus with increased loading of liquid fillers compared to the measured modulus for PDMS film was evident from the plot. The equations predict a Young's modulus of ~0.747 MPa for 20% filler loading compared to the 1 MPa for pristine PDMS film.

Schematic of composites

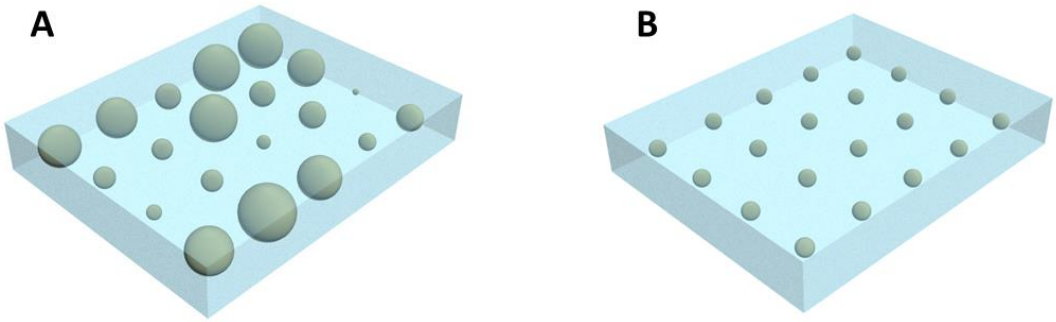

Figure S2. (a) Schematic of expected non-uniform filler distribution and random filler size distribution in the fabricated composite of Water and PDMS. (b) Schematic of expected uniform filler distribution and smaller average filler size in the fabricated composite of EMIMTFSI and PDMS.

Effect of type of filler on mechanical properties

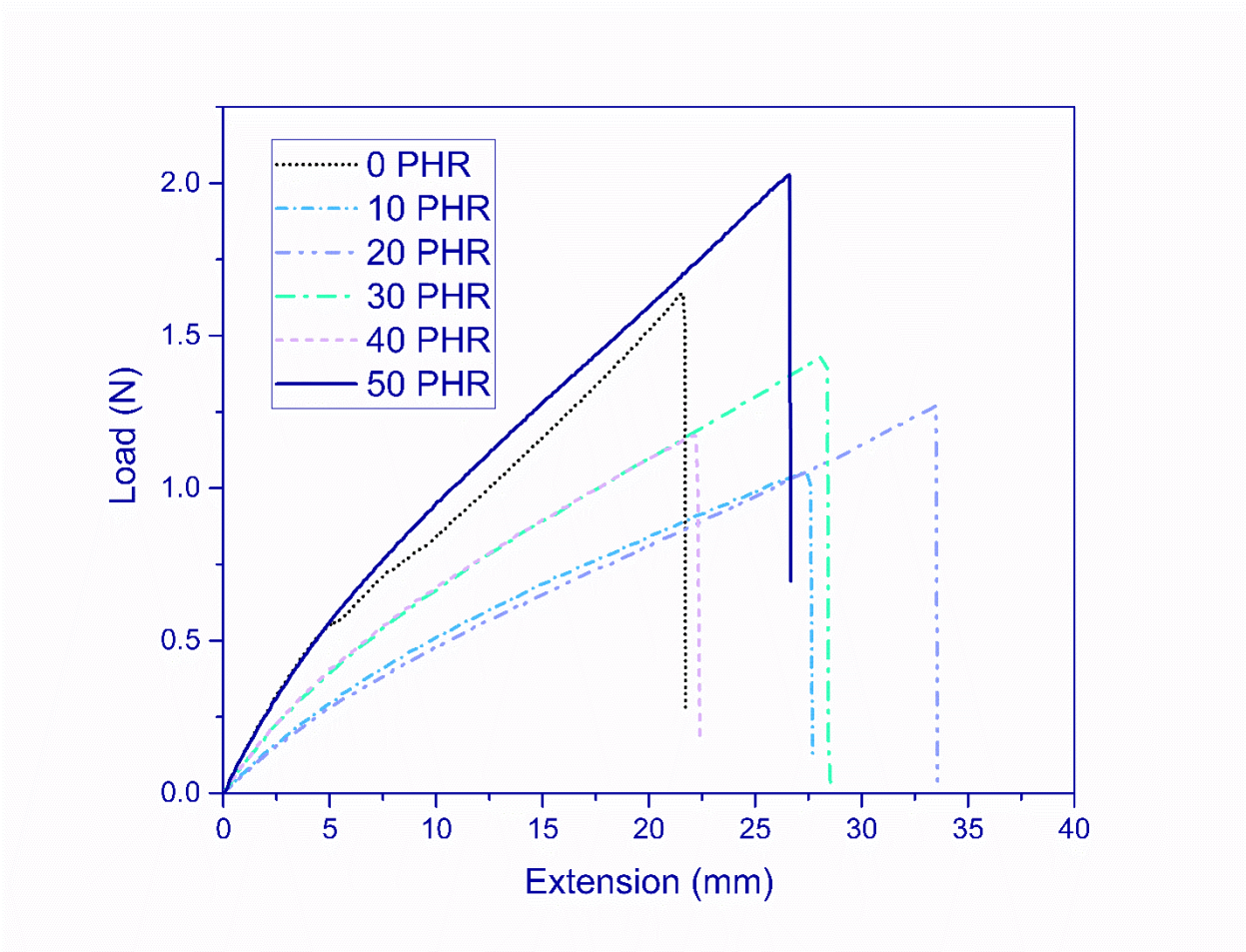

Figure S3. Stress-strain curves for Water-PDMS composites for different volume loading of water. PHR stands for parts of water (by volume) per hundred parts of the PDMS (by volume). Unpredictable mechanical properties are observed and can be attributed to non-compatibility between the filler and the matrices.

Globular filling structures resisting tension

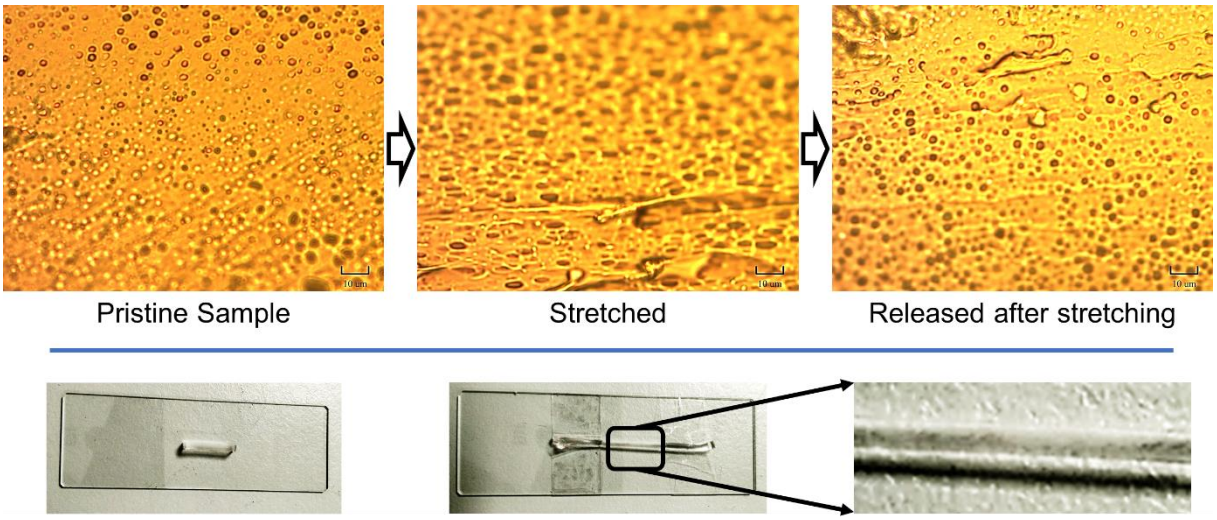

Figure S4. Stability of self-enclosed globules on EMIMTFSI inside PDMS matrix under large stretching. (Scalebar – 10µm) As evident from the optical microscopy images, the globules elongate along the direction of applied stretch without getting destroyed. After the stretched film is released, the globular phases can be observed without any apparent damage. Bottom row images depict the pristine sample, stretched sample (fixed in place by tape) and a zoomed-in image of the stretched sample indicate no leakage of EMIMTFSI.

Globular filling structures resisting compression

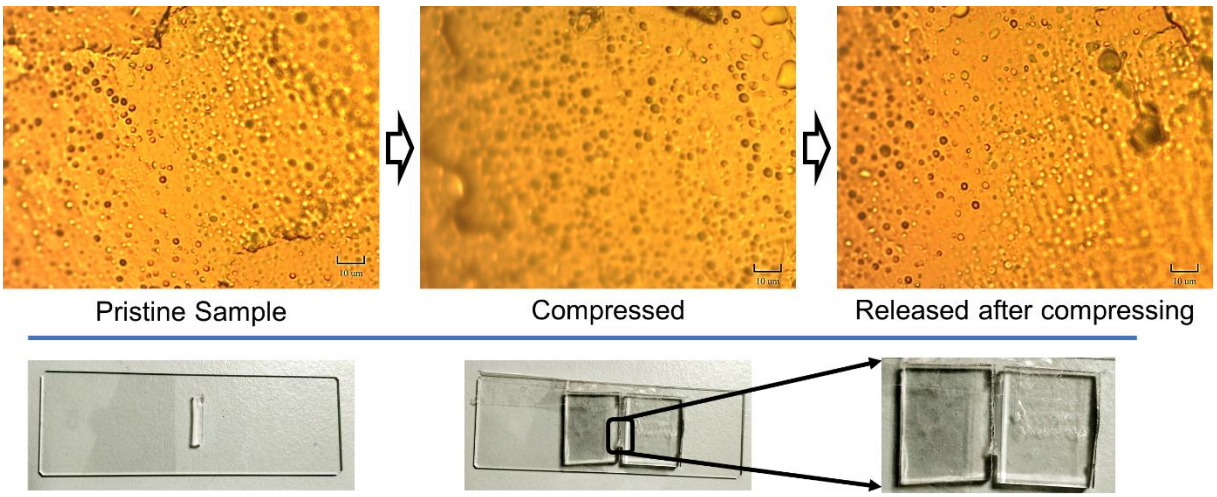

Figure S5. Stability of self-enclosed globules on EMIMTFSI inside PDMS matrix under compression. (Scalebar – 10µm) As evident from the optical microscopy images, the globules get closely packed when compressed, without getting destroyed. After the compressed film is released, the globular phases can be observed without any apparent damage. Images of pristine sample, compressed sample and zoomed-in image of compressed sample to show no leakage of EMIMTFSI.

Optical microscopy images

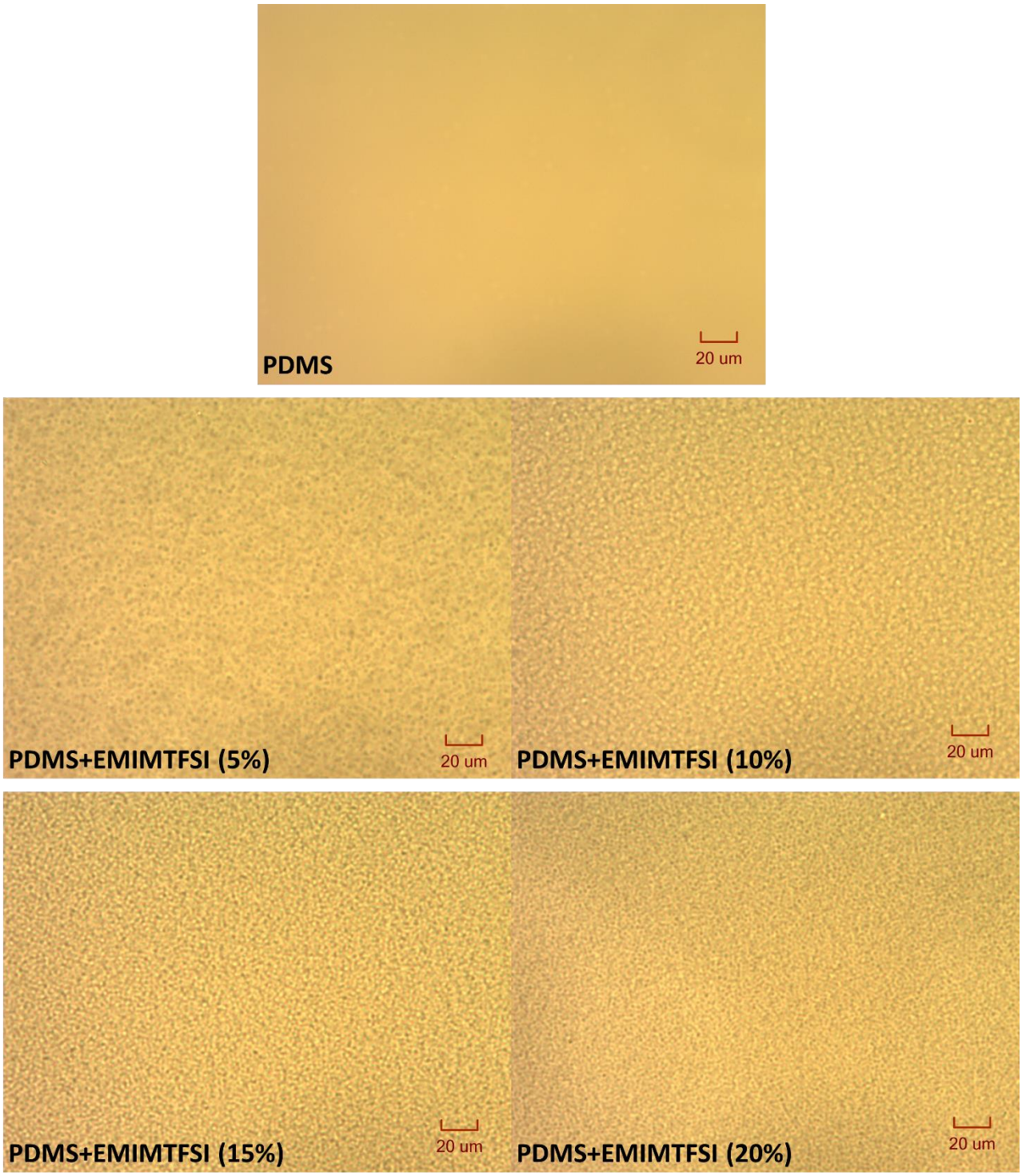

Figure S6. Optical microscopy image for pristine PDMS, PDMS+EMIMTFSI (5%), PDMS+EMIMTFSI (10%), PDMS+EMIMTFSI (15%) and PDMS+EMIMTFSI (20%).

FTIR spectroscopy

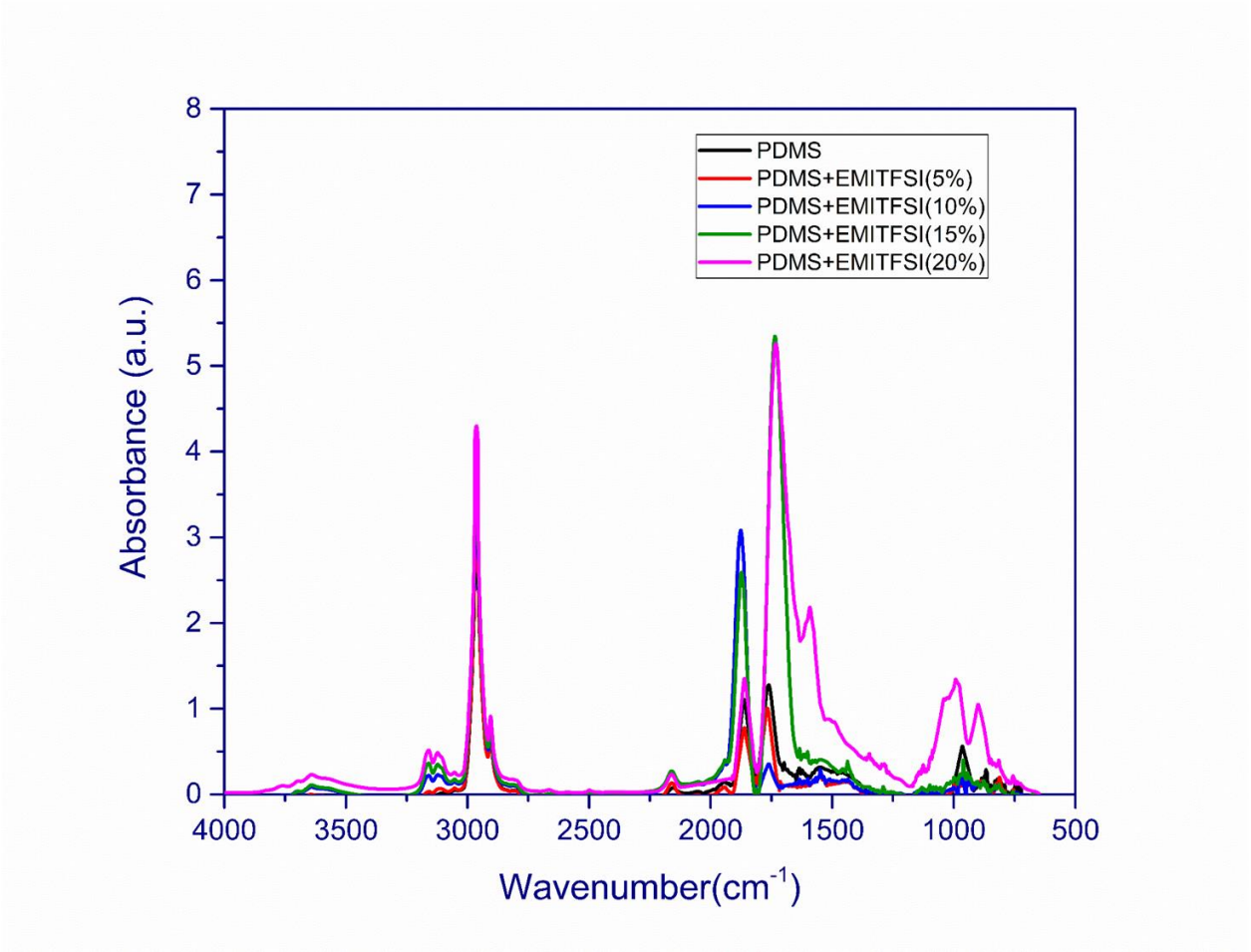

Figure S7. Fourier-transform infrared spectroscopy of pristine PDMS and EMIMTFSI-PDMS composites with different filler concentrations. Different peaks originating in the infrared spectrum compared to the pristine PDMS matrix are characteristic peak of EMIMTFSI and cements the proof of presence on EMIMTFSI phases in the PDMS matrix.

Electric circuit equivalent of DEA

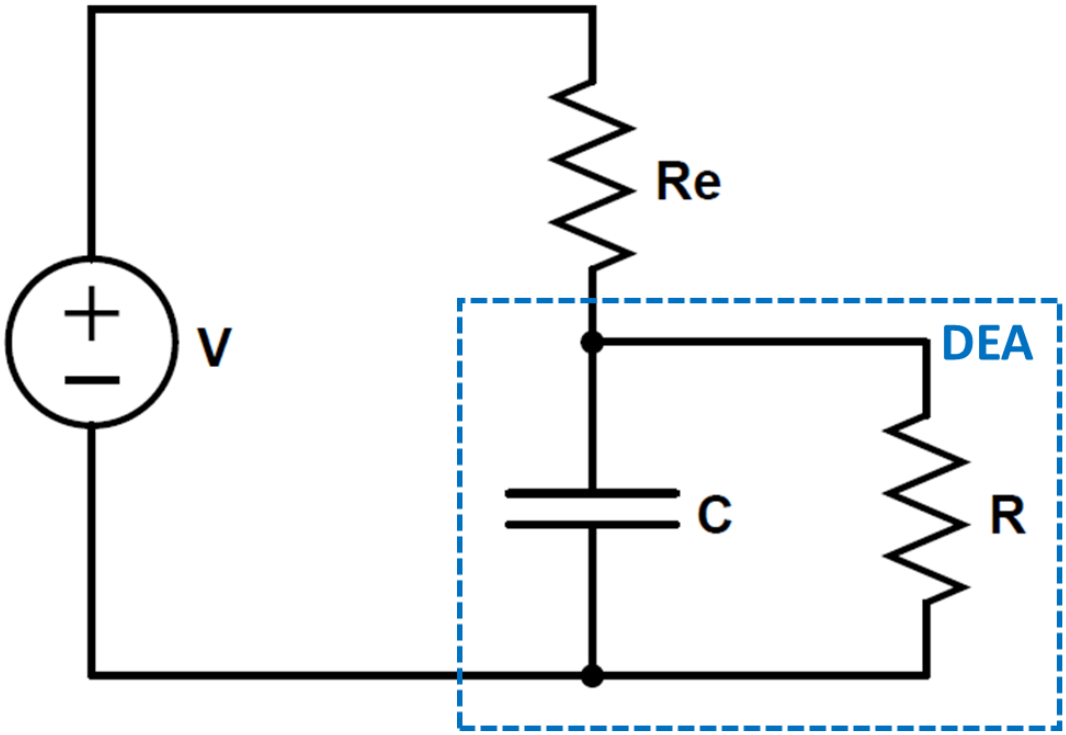

Figure S8. Equivalent circuit model for a DEA, where the DEA has been modelled as a capacitor in parallel to a resistance. The capacitor denotes the energy storage component of the dielectric, given by the real part of the permittivity (ε') and provides the k-value (dielectric constant) for the dielectric. Resistor denotes the energy dissipation component of the dielectric and is given by the imaginary part of the permittivity (ε"). Consequently, complex permittivity is plotted as a simple vector diagram with real and imaginary components at 90^{o} to each other (out of phase).

Effect of electrode area on relative permittivity (dielectric constant)

Capacitance is given by the formula in equation (9), where ε_o is the permittivity of vacuum, ε_r is the relative permittivity (dielectric constant) of the elastomer, A is the area of the electrodes and d is the thickness of the elastomer.

$$C = \varepsilon_o \varepsilon_r \, {}^{A}/_{d} \qquad (9)$$

For the same thickness of the material, capacitance increases proportionally with the area of the electrodes, given that the dielectric constant remains unchanged.

To understand the effect of area of composite under consideration on the measured dielectric behavior, capacitance measurement was done for 2 electrode areas. Figure S9 shows the plot of capacitance (per unit area) with varying frequency for different areas of the electrode. Using equation (9) to calculate the ε_r values (@ 1 kHz), we get the values to be ~ 6.44 (for 1 cm square) and ~ 6.29 (0.5 mm square). This is a slight variation from the dielectric constant measured for larger area (~ 6.9) (Figure 3a). This variation could be attributed to difference in measuring instruments (LCR meter for smaller area samples and dielectric spectrometer for large area sample) and measuring environment (shielding for large area samples).

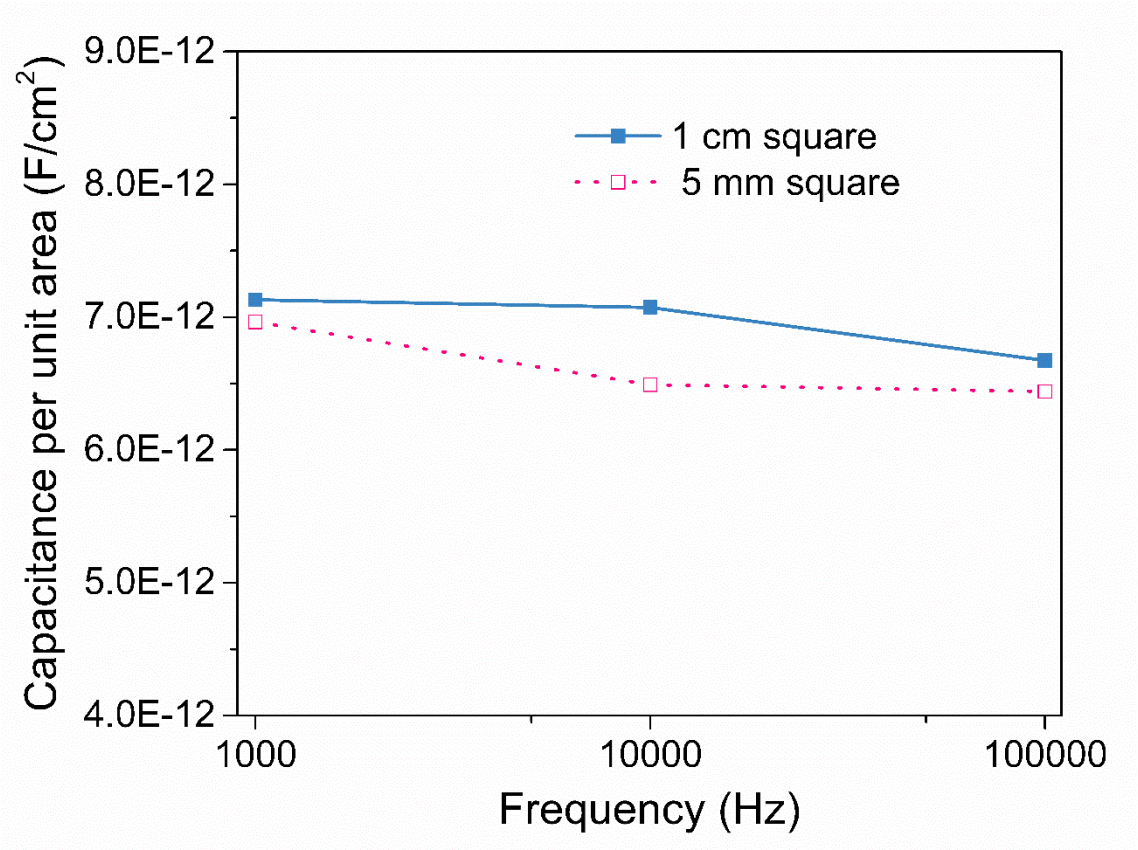

Figure S9. Capacitance (per unit area) measured at different frequencies (using LCR meter) for 0.8 mm thick PDMS+EMIMTFSI (20%) composite for different electrode sizes. (Square with 1 cm side and square with 0.5 mm side)

Figure of merit

Figure of merit (F.O.M.) was estimated using the equation employed by Romasanta et. al. for composites.

$$F.O.M. = {}^{Y_o \varepsilon_c'}/_{Y_c \varepsilon_o'} \quad (9)$$

Where Y_o and Y_c are the Young's modulus of the elastomer matrix and composite matrix respectively, and ε'_o and ε'_c are real part of relative permittivity for the elastomer matrix and the composite matrix respectively.

Table S1. Figure of merit calculated for PDMS-EMITFSI composites and comparison to solid filler systems.

Composites		**Dielectric Constant, ε' at 1kHz**	**Young's Modulus, *Y* (MPa)**	**Figure of Merit**	**Reference**
Elastomer Matrix	**Filler**				
SEBS-g-MA (poly-styrene-co-ethylene-co-butylene-co-styrene-g-maleic anhydride)	Polyaniline (PANI)	63.0	3.986	***35.8***	Stoyanov et al.
Polydimethylsiloxane (PDMS)	Calcium Copper Titanate (CCTO) $CaCu_3Ti_4O_{12}$	5.22	0.58	***1.64***	Romasanta et al.
Acrylic rubber (ACM)	Barium titanate ($BaTiO_3$) and Carbon Black	40.5	2.62	***1.60***	Poikelispää et al.
Polydimethylsiloxane (PDMS)	EMITFSI	6.27	0.02	***84.73***	**This Work** - Uneven Mixing (25 vol%)
Polydimethylsiloxane (PDMS)	EMITFSI	6.93	0.01	***187***	**This Work** - Even Mixing (20 vol%)

Effect of film thickness on mechanical and dielectric properties

As the thickness of the film was varied, the dielectric constant was calculated to be similar (@ 1 kHz). The dielectric constant values were calculated to be 6.44 (0.8 mm thick film) and 6.48 (0.5 mm thick film), from the capacitance values. There is a slight variation with respect to ~2 mm thick films and could be due to different measuring equipment and measuring environment.

A trend is observed with varying thickness in the observed stress-strain curves as well (Figure S). As the thickness increases, the material appears to get slightly softer and more stretchable. Young's modulus was calculated to be 20 kPa for 0.75 mm thick film, 10 kPa for 1.45 mm thick film and 5 kPa for 2.25 mm thick film. Ultimate strain at break increased from 371% (0.75 mm) to 435% (1.45 mm), increasing further to 507% for 2.25 mm thick film.

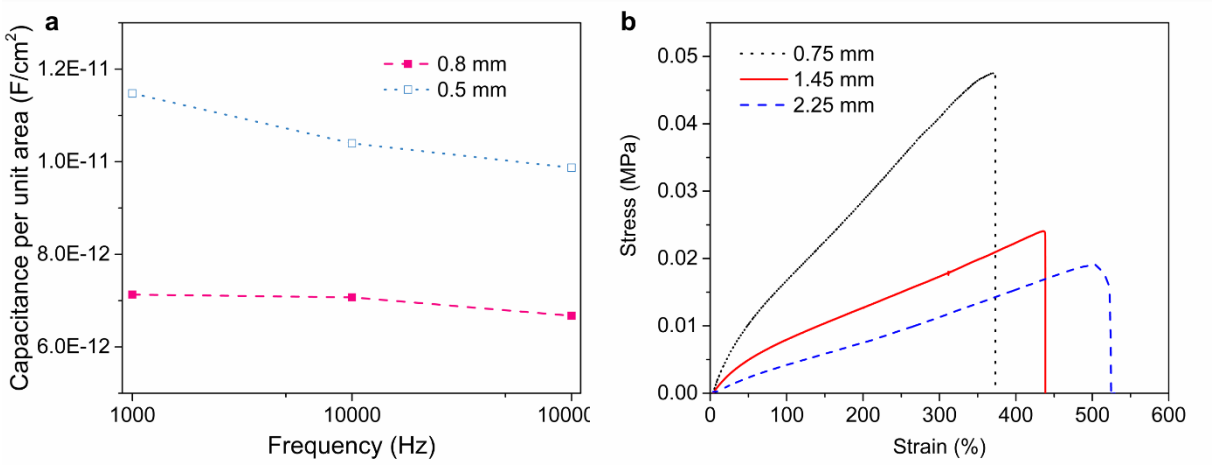

Figure S10. (A) Variation in capacitance with thickness of the film for PDMS+EMIMTFSI (20%) composite. (B) Stress-strain curve obtained for PDMS+EMIMTFSI (20%) composite for varying film thickness.

Electrical breakdown in PDMS+EMIMTFSI (20%) composite

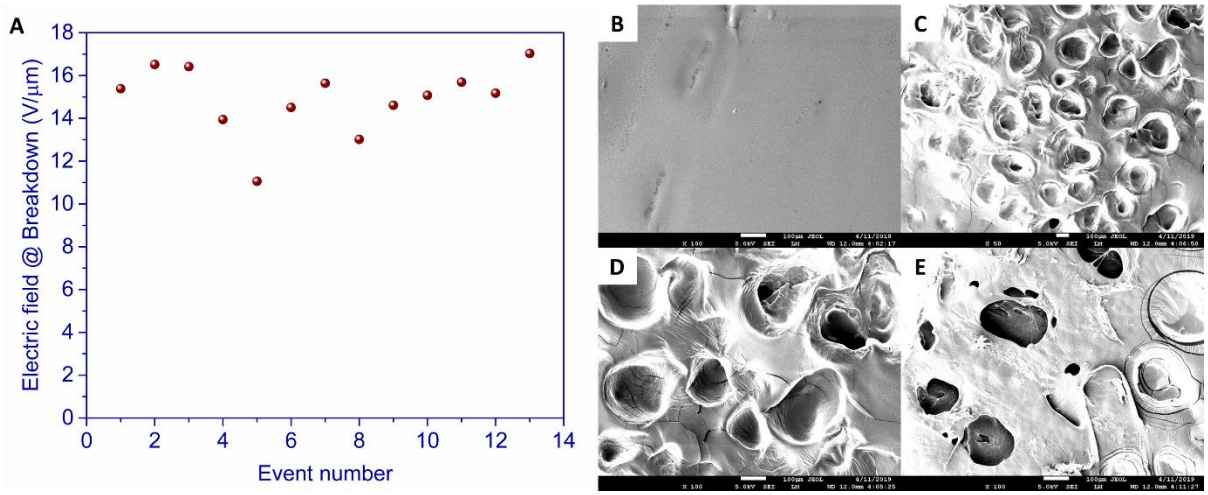

Figure S11. Electrical breakdown on EMIMTFSI-PDMS composites. (A) Electrical breakdown measurements for 100 microns thick PDMS+EMIMTFSI (20%) composite showing a low breakdown strength. (B) SEM image of the top surface of a PDMS+EMIMTFSI (20%) composite film. SEM images ((C), (D) & (E)) showing the breakdown of the PDMS+EMIMTFSI (20%) composite under applied electric field.

Thermogravimetric analysis – onset temperature

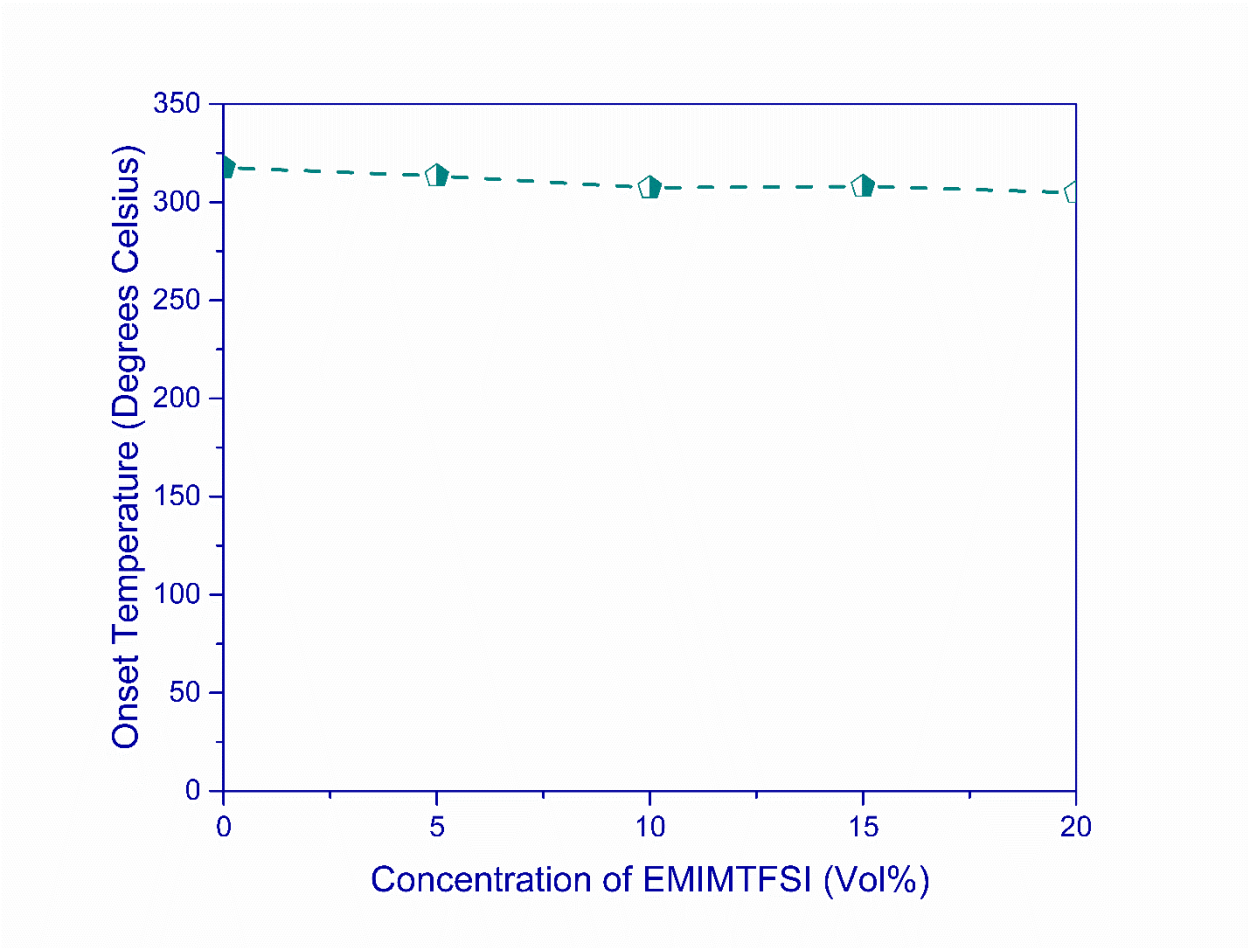

Figure S12. Plot of Onset temperature (2% weight loss) versus concentration of EMIMTFSI.

Effect of water content on mechanical properties of PAAM hydrogels

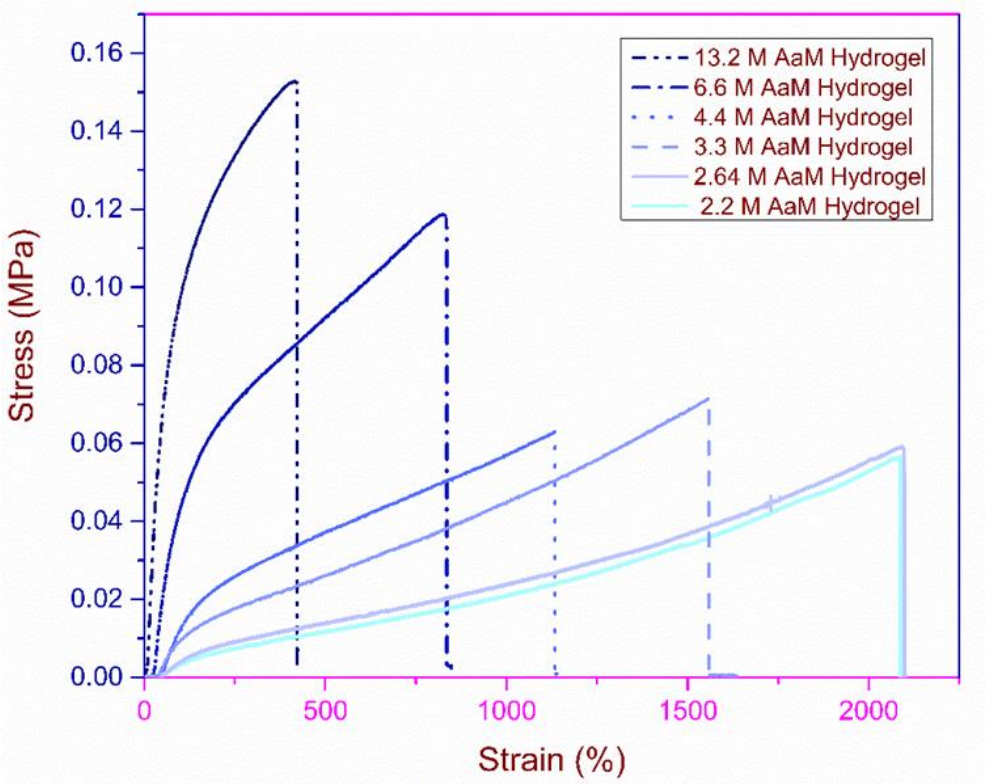

Figure S13. Stress against strain for six different concentrations (molarities) of acrylamide (AaM) monomer in the hydrogel network. Molarity of acrylamide (AaM) is varied by keeping the polymer concentration constant and varying the content of water. A ratio of higher water content to lower monomer concentration leads to lower elastic modulus and higher ultimate strain in the resulting hydrogel. Young's modulus is observed to decrease from 0.21 MPa to 0.6 kPa as the water concentration increases from 2.5 ml to 30 ml (and molarity of AaM decreases from 13.2 M to 2.2 M). This decrease in Young's modulus is also accompanied with an increase in the stretchability of the matrix; with an ultimate strain measured at ~400% for 13.2 M AaM hydrogel and ~2100% for 2.2 M AaM hydrogel.

Effect of thickness of PDMS+EMIMTFSI (20%) film on transmittance

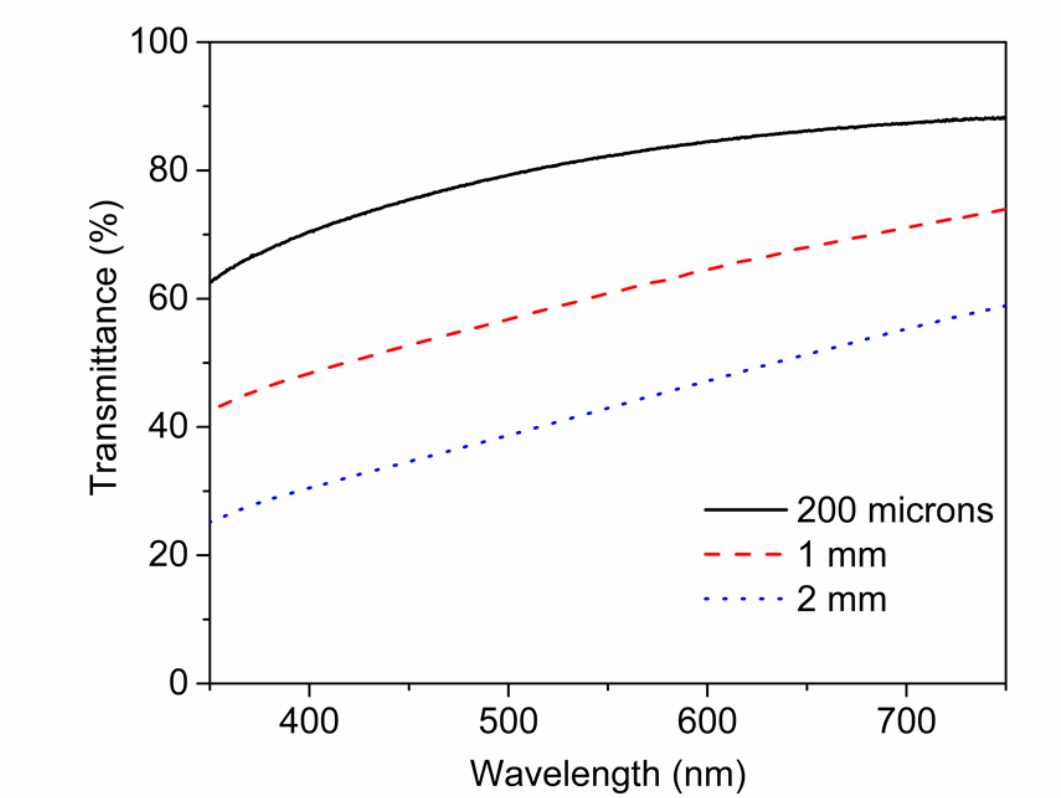

Figure S14. Transmittance versus wavelength plot (from the UV-Vis measurements) for PDMS+EMIMTFSI (20%) composite with varying film thickness. As the film thickness increases, the transmittance decreases.

Hysteresis free performance of pressure sensor while sequential loading and unloading

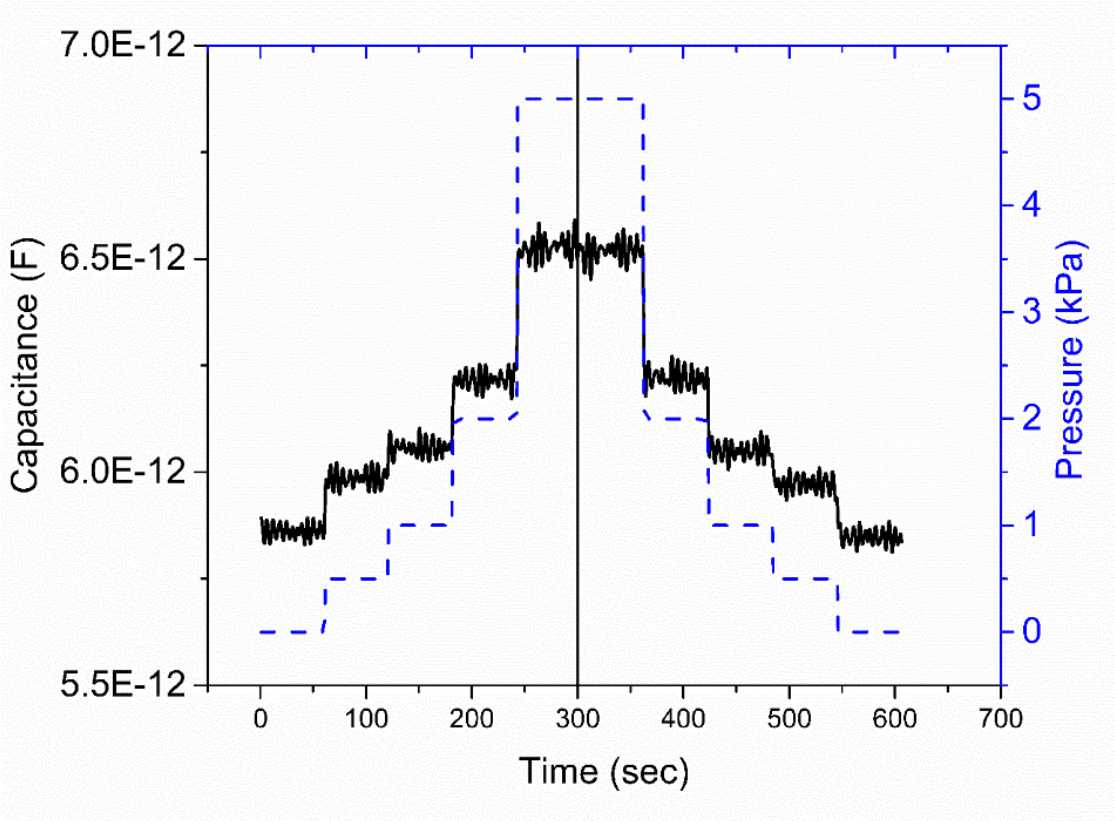

Figure S15. Sequential loading and unloading of the weights on the capacitive pressure sensor (1 cm^2 area; 2.5 mm thickness) fabricated using PDMS+EMIMTFSI (20%) composite showing no observable hysteresis. This is further proof of stable nature of liquid fillers inside the matrix and non-hysteresis observed in stress-strain curves.

Actuation performance: actuation strain versus applied voltage

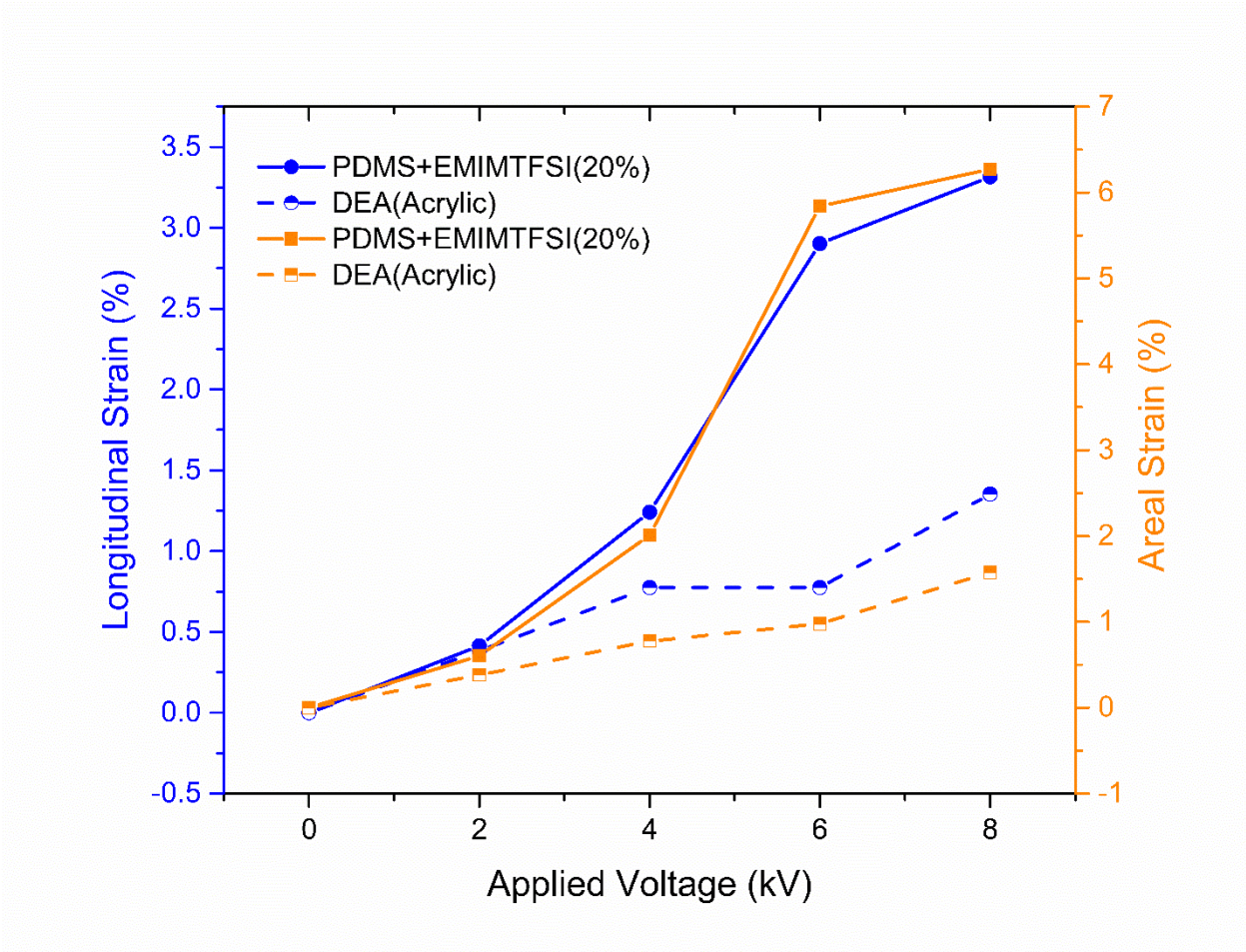

Figure S16. Longitudinal and areal strain against applied voltage for PDMS+EMIMTFSI (20%) composite and acrylic (VHB 4910). PDMS+EMIMTFSI (20%) composite shows ~2.5 times improvement in longitudinal strain compared to commercially available acrylates (VHB 4910) at same voltage. PDMS+EMIMTFSI (20%) (6.27%) show 4 times improvement in areal strain compared to commercially available acrylates (VHB 4910) (1.58%).

Cyclic actuation performance

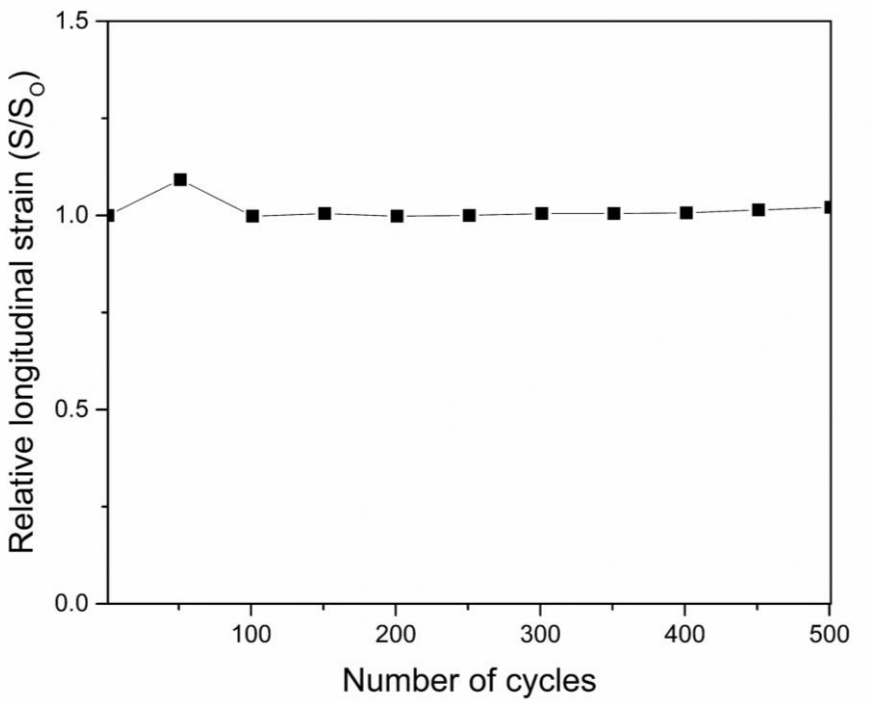

Figure S17. Relative longitudinal strain produced with number of cycles. The actuator maintains its performance for 500 cycles without any deterioration.

SEM Image of top and bottom surface

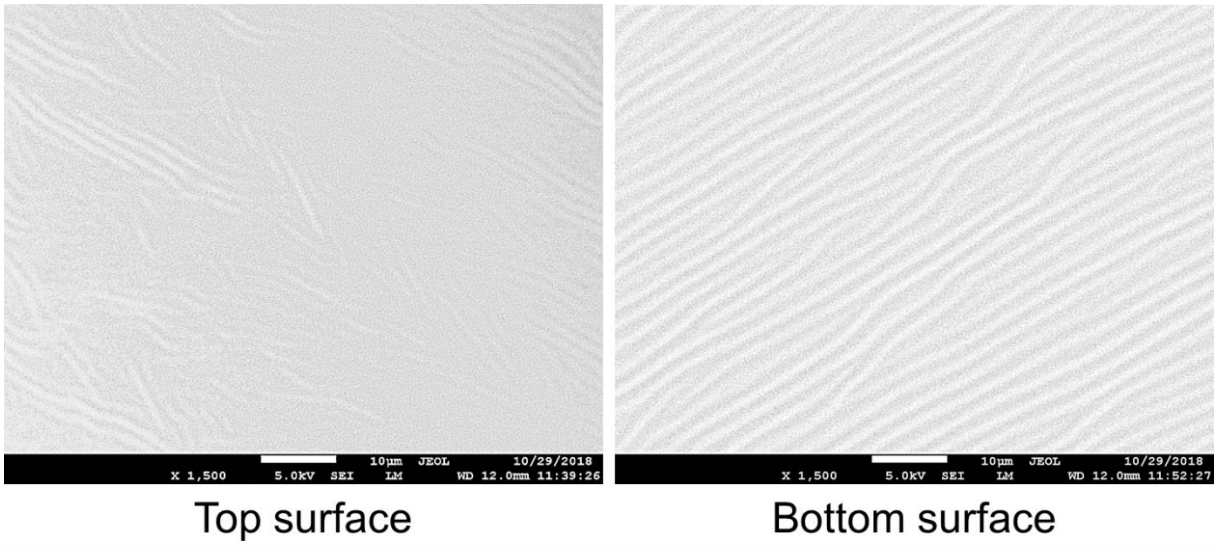

Figure S18. Scanning electron micrographs of top and bottom surface of the PDMS+EMIMTFSI (20%) composites. It is evident from the SEM images that the fillers are enclosed within the matrix and do not migrate to the surface of the composite.

Effect of filler size distribution on electromechanical properties

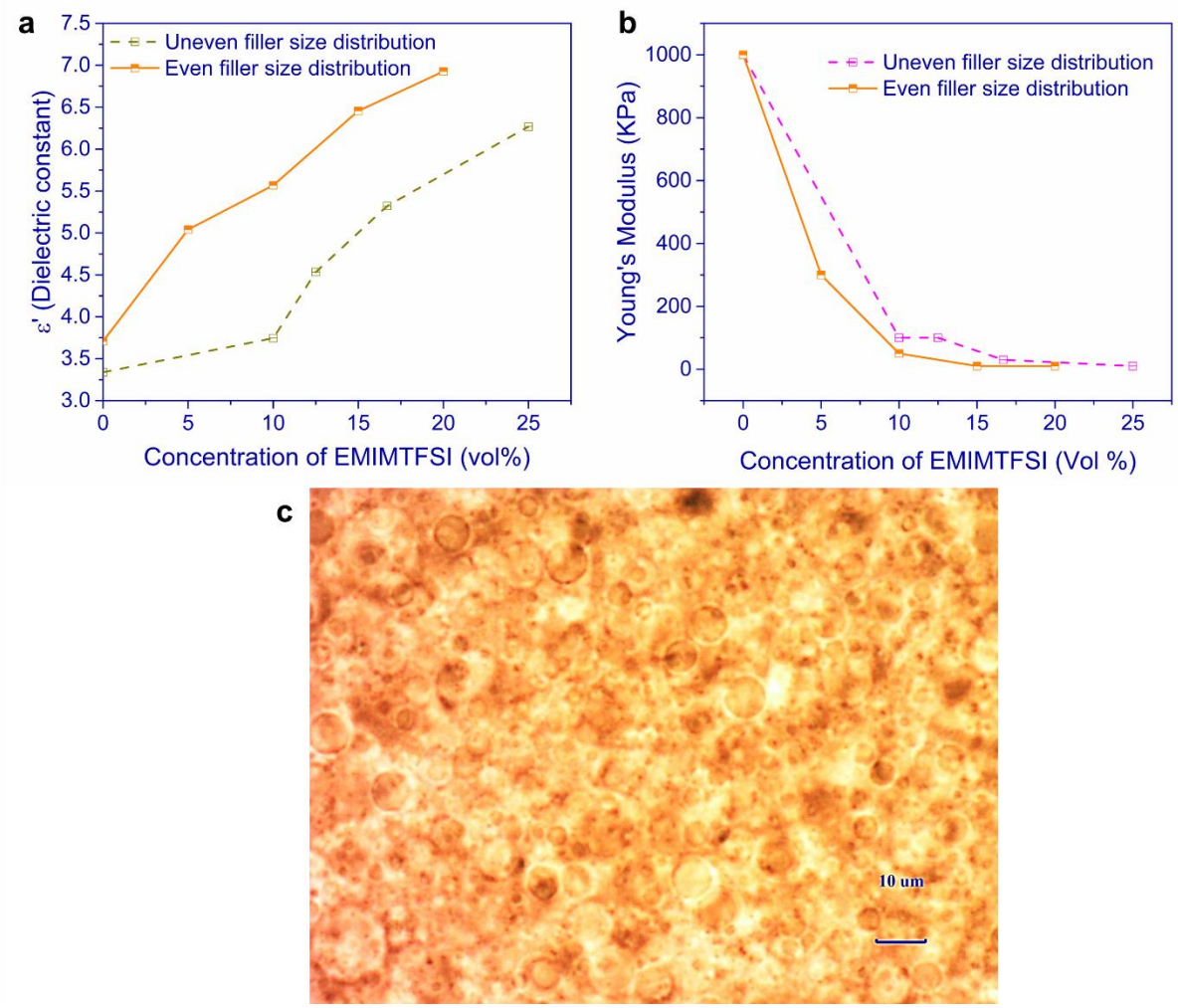

Figure S19. (a) Effect of filler size distribution on the real part of the permittivity (dielectric constant, @1kHz) of EMIMTFSI-PDMS composites with different filler concentrations. (b) Effect of filler size distribution on the Young's modulus of the resulting composite matrix with varying filler loadings. (c) Optical microscope image of PDMS+EMIMTFSI (25%) fabricated via hand mixing, showing uneven filler size distribution.